Nature and Measurements of Torque Ripple of Permanent-Magnet Adjustable-Speed Motors

John S. Hsu (Htsui), Brian P. Scoggins, Matthew B. Scudiere, Laura D. Marlino, Donald J. Adams, Pragasen Pillay
Senior Member *Senior Member*

Oak Ridge National Laboratory
P.O. Box 2003, K-1220, MS 7280
Oak Ridge, TN 37831-7280

Faculty Research
Participant
University of New Orleans

Abstract: **Torque ripple of permanent-magnet motors can be classified into four types depending on the nature of their origin. The four types are pulsating torque, fluctuating torque, reluctance cogging torque, and inertia and mechanical system torque.**

Pulsating torques are inherently produced by the trapezoidal back-emf's and trapezoidal currents used in certain permanent-magnet adjustable-speed motors. The torque ripples caused by pulsating torques may be reduced by purposely produced fluctuating counter torques.

Air-gap torque measurements are conducted on a sample motor. Experimental results agree with theoretical expectations.

I. Introduction

Torque ripple of adjustable speed permanent-magnet (PM) motors have adverse effects in many applications. For example, low surface finish roughness for machine tool drives depends on motor torque quality. For propulsion and vehicle motors, quietness and smoothness are strongly required.

The severity of torque ripple increases at low speeds. In addition, the effect of the moment of inertia that tends to absorb shaft speed variations is less significant at lower rate of speed fluctuations. A smooth air-gap torque is particularly desired at low speed.

There are various inverter and motor schemes for permanent-magnet adjustable-speed drives [1-6, 11-17]. Most existing literature studies motors having surface-mounted magnets. A minor portion of the literature studies buried magnets [1, 2, 3].

The cogging torque of a PM motor is produced by non-uniformly distributed air-gap permeance associated with the teeth and the permanent magnets. Skewing either the teeth or the magnets is one approach for cogging-torque reductions [3]. It is also possible to reduce the cogging torque by properly choosing the ratio of magnet width to slot pitch without skewing [4]. Other approaches, such as tapering the magnet edges, may also reduce cogging torques.

The air-gap torque in Newton meters of a PM motor is

$$T = \frac{i_a e_a + i_b e_b + i_c e_c}{2\pi \frac{(speed)}{60}} \qquad (1)$$

where e_a, e_b, and e_c are the back electromotive forces (emf's) induced in the armature windings by permanent-magnets, while i_a, i_b, and i_c are the armature currents. The rotor speed is given in revolutions per minute (rpm).

Various data-signal-processing (DSP) approaches are possible for controlling the constant air-gap torque presented by equation (1). When it is assumed that e_a, e_b, and e_c are not changed under various loads, either the dc-link current or the armature currents can be adjusted to change i_a, i_b, and i_c. The latter approach [5] may reduce torque ripples caused by commutation.

When saturation effects are considered in PM motors, Chen, Levi, and Pelka [6] suggest that the field excitation voltages of PM alternating-current (ac) motors can be considered constant at their open circuit values for all points of operation. On the other hand, Ostovic and Osijck [1] use a flux tubes method to evaluate transient states in a PM machine. The nonlinear characteristics of the induced voltages and the torque are calculated.

Most existing literature on the torque ripple of PM motors appears to be theoretical investigations. Few studies conduct tests, and laboratory torque measurements are generally not included.

DISCLAIMER

DISCLAIMER

Portions of this document may be illegible in electronic image products. Images are produced from the best available original document.

This paper looks into the origin of four types of torques that are components of torque ripple of adjustable-speed PM motors. Experimental results obtained from laboratory air-gap torque measurements agree with theoretical expectations.

II. Spatial and Time Harmonics

The armature windings and the permanent magnets of PM motors generally contain spatial harmonics, and their armature currents have time harmonics.

A. *Winding Spatial Harmonics*

The motor windings of a phase are normally situated in particular slots. For three-phase windings, each phase winding is located 120 electrical degrees apart from the others. The fundamental a-, b-, and c-phase-winding locations follow a sequence that is in the same direction as the normal shaft rotation. This sequence is called the positive sequence.

If a current is flowing through the winding, the magnetomotive force (MMF) generated is not a pure sine wave. Each slot has a certain concentration of ampere-turns that produces a discrete change of MMF from its adjacent teeth. The MMF wave of the winding contains fundamental and harmonic components. These components represent the existence of winding spatial harmonics. In practice, the winding spatial harmonics are calculated through winding factors [7]. The values for an experimental motor used later are listed in Table 1.

No. of poles=4		
No. of stator slots=24		
Double-layer winding, 60-degree phase belt		
Coil pitch=1 - 6		
Spatial stator-winding harmonics:		
Order of harmonics, n	Winding factor, K_n	Relative sequence of three phases
1	0.93	Positive
3	0.50	Zero
5	0.07	Negative
7	0.07	Positive
9	0.50	Zero
11	0.93	Negative

Table 1 Spatial stator-winding harmonics

Although phase windings are located in positive sequence, their individual harmonic windings may be located in either positive, negative, or zero sequence, where the negative sequence is in the opposite direction to the positive sequence. Zero sequence means that the three-phase harmonic winding components are located at the same positions.

The harmonic windings having numbers of poles proportional to their harmonic orders are connected in series. For example, the fifth spatial stator-winding harmonic component shown in Table 1 represents a 20-pole winding connected in series with the 4-pole fundamental winding. For three phase windings, the locations of the 20-pole harmonic windings are in negative sequence. With reference to their winding factors, the significance of the 20-pole harmonic windings viewed from the winding terminals is 7% of the fundamental winding component.

B. *Spatial Harmonics of Permanent-Magnets Flux*

The rotor of the experimental motor has four surface-mounted permanent magnets The pole span of each magnet is 140 electrical degrees. The spatial harmonics of a trapezoidal wave having a 140 electrical-degree-wide plateau are:

Order of harmonics: 1 3 5 7 9 11

Relative amplitudes: 100% 31% 13% 4% 0% 2%.

The spatial harmonics of the rotor PM flux are rotating in the positive direction at the rotor mechanical speed.

C. *Back emf Induced by Permanent Magnets*

When the spatial harmonics of the PM rotate in the air gap at the rotor speed, the emf magnitudes and frequencies induced in the stator winding depend on the individual winding spatial harmonics. An emf of a particular harmonic order is induced only when both the stator winding harmonic component and the rotor PM flux spatial harmonic component are of the same order. Table 2 shows the relative frequencies of the back emf's of the sample windings given in Table 1 with the above sample spatial harmonics of PM flux.

Back emf's induced by permanent magnets		
Order of harmonics	Relative amplitude	Relative frequency
1	100%	1ω
3	17%	3ω
5	1%	5ω
7	<1%	7ω
9	0%	9ω
11	2%	11ω

ω_ Fund. electrical angular frequency

Table 2 Back emf's induced by PM of experimental motor

D. *Time Harmonics of Armature Currents*

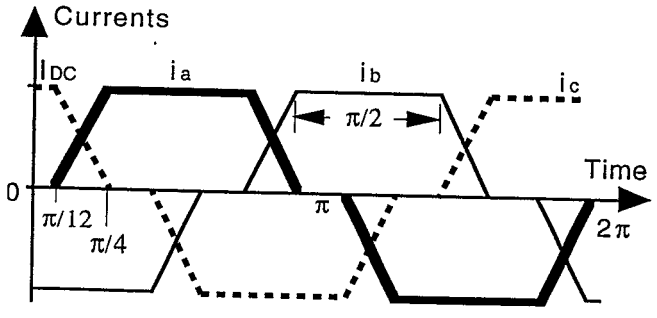

Fig.1 Sample trapezoidal armature currents

Trapezoidal armature-current harmonics		
Order of harmonics	Relative amplitude	Relative sequence of three phases
1	100%	Positive
3	0%	Zero
5	15%	Negative
7	8%	Positive
9	0%	Zero
11	1%	Negative

Table 3 Time harmonics of trapezoidal currents of Fig. 1

As an example, the time harmonics of a trapezoidal armature current shown in Fig. 1 are listed in Table 3. The relative sequences indicate the phasal relationships in time among three phases.

III. Nature of Torque-Ripple Originations

Torque ripple has four origins, which are classified as follows:

A. Pulsating Torques

This type of torque is usually the most common in PM motors. Pulsating torque originates from the interaction between stator and rotor fields. In order to produce a pulsating torque the following conditions must be met:

1) The stator field and the rotor field have an identical number of poles. Fields having different numbers of poles do not interact with each other.

2) The stator field and rotor field are rotating at different speeds. One field may be stationary, or both may rotate in either the same or opposite directions.

3) The frequency of the pulsating torque is the difference of the rotating speeds per second of the stator and rotor fields

For example, the three phase currents of the 5th time harmonic given in Table 3 are in negative sequence. When these currents go through the fundamental winding component shown in Table 1, a 4-pole rotating field at five times the rotor speed but in a reversed direction is generated. The interaction of this field with the fundamental forward-rotating field of the rotor produces a sixth order of pulsating torque. The torque magnitude is proportional to the product of the rotor fundamental field magnitude, the stator 5th order winding factor, and the relative amplitude of the 5th harmonic of the armature current. Other orders of pulsating torques can be evaluated in like manner.

If the steady air-gap flux distribution is spatially sinusoidal and the armature steady input currents are sinusoidal in time, the motor does not yield pulsating torque components.

B. Fluctuating Torques

Torque fluctuations can be produced by altering the magnitudes of phase currents in the same ratio. The sample DSP approach discussed earlier is an example of using torque fluctuations for torque ripple elimination.

In a given motor the back emf is fixed and torque and torque ripple can only be regulated by maintaining the proper instantaneous current in each of the three phases. Since the operating voltage and the switching time intervals are bounded, current regulation cannot be exact or in some cases may not even be close to the desired value. This occurs at the higher end of the operating speed where the back emf is large compared to the driving voltage. When the inverter switch is set to increase the current, the charging voltage across the motor inductance is the driving voltage minus the back emf. In this region the resultant voltage can be too small to build current fast enough. When the inverter switch is set to reduce the current, the back emf adds to the link voltage and can discharge the current in a phase significantly faster than the charging rate. With a Y configuration requiring the phase currents to sum to zero, the interaction of the three phases along with the difference in charging and discharging makes it impossible to completely regulate each phase current precisely at all times in the higher operating speed regions without increasing the source voltage. But at the lower speeds with the switching times bounded this higher source voltage can cause large current fluctuations and therefore produces significant torque ripple at the switching rate.

C. Reluctance Cogging Torque

Armature teeth present non-uniformly distributed air-gap reluctance. The reluctance torque produced by teeth and permanent magnets varies as their relative positions change. This torque can be felt while turning the motor shaft by hand without energizing the motor. The cogging torque versus shaft position can be measured in a similiar manner. Different approaches for cogging torque reductions can be found in the literature.

D. Inertia and Mechanical-System Torques

When the speed of the rotor is changed, a torque proportional to the product of its moment of inertia and the rate of speed change is generated. This torque resists the change of speed. The moment of rotor inertia acts like a filtering capacitor in an harmonic-prone electronic circuit.

At low speed, the rate of speed ripple is lower. Subsequently, this torque is weaker. The mechanical components of the motor can be considered as a spring system. Certain torques are generated according to the dynamic motions of the spring system.

IV. Air-Gap Torque of Three-Lead, Three-Phase Motors

Air-gap torque equations using measurable data have been known for several decades [8-10, 18, 19]. One familiar expression [8] is presented in (2).

Equation (3) is rewritten [9] from (2) for the line data as depicted in Fig. 1, where the symbols are denoted by their

corresponding line identifications in the suffixes.

$$Torque\ [Nm] = \frac{p \cdot \sqrt{3}}{6} \left\{ \begin{array}{l} i_a(\psi_c - \psi_b) \\ +i_b(\psi_a - \psi_c) \\ +i_c(\psi_b - \psi_a) \end{array} \right\} \qquad (2)$$

where suffixes a, b, and c stand for phase values,

p is number of poles, i represents current,

and ψ is for flux linkage.

$$Torque\ [Nm] = \frac{P}{2 \cdot \sqrt{3}} \left\{ \begin{array}{l} -(i_A - i_B) \cdot \int [v_{CA} - R(i_C - i_A)]\, dt \\ +(i_C - i_A) \cdot \int [v_{AB} - R(i_A - i_B)]\, dt \end{array} \right\} \qquad (3)$$

Equation (3) is valid for either Y- or delta-connected motors, where

i_A, i_B, and i_C = line currents
R = half of the line-to-line resistance value.

From the definition of R, the following two expressions are for Y and delta-connected motors, respectively.

R = phase resistance, r, for Y-connected motor
R = r/3 for delta-connected motor.

Equation (3) contains certain errors due to the following assumptions and simplifications. First, the three-phase leakage reactances are linear and identical. Second, the negative sequence winding (not supply) components are negligible. Third, the torque components produced by sources that are not dependent on the armature winding currents, such as permeance cogging torque in a permanent-magnet motor, are not considered. Fourth, the instantaneous magnetic unbalances [10] for three phases are ignored. Fifth, the effect of dc components in the flux linkages are neglected. Finally, the equations are not affected by minor speed ripples.

When using either three leads for Y-connected motors without a neutral connection or three leads for delta-connected motors, (3) can be further simplified by using $i_B = -(i_A + i_C)$. The above equation can be rewritten to the known format that uses only two line voltages, two line currents, and one-half of the line-to-line resistance as the input data for the calculation of the air-gap torque.

$$Torque\ [Nm] = \frac{P \cdot \sqrt{3}}{6} \left\{ \begin{array}{l} -(2 \cdot i_A + i_C) \cdot \int [v_{CA} - R(i_C - i_A)]\, dt \\ +(i_C - i_A) \cdot \int [-v_{BA} - R(2 \cdot i_A + i_C)]\, dt \end{array} \right\} \qquad (4)$$

V. Air-Gap-Torque Measurements

A. Experimental Setup

The experimental setup is shown in Fig. 2. Isolated current and voltage transducers are used. Isolated transducers are advantageous since the signals can be connected to a single common point. This is a great convenience to the data acquisition system provided that additional instrumentation errors are negligible.

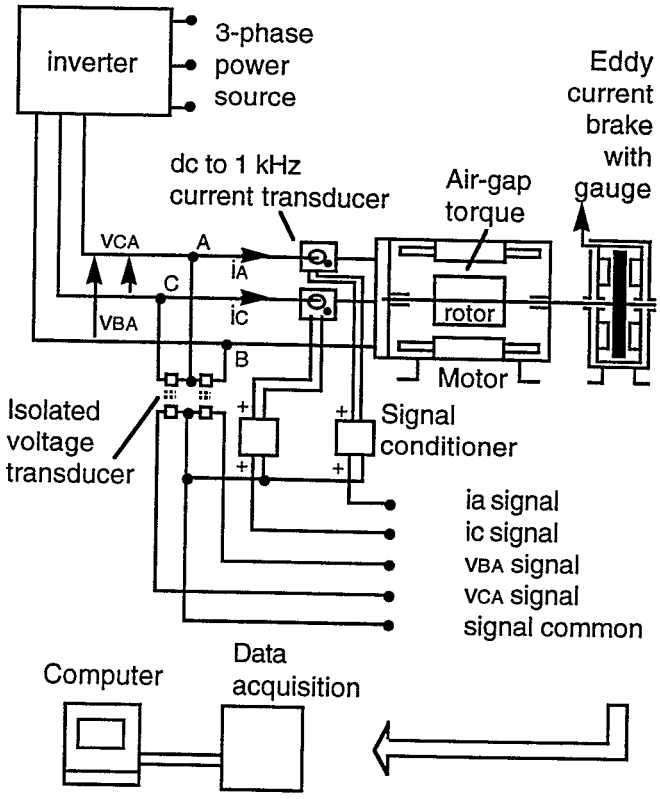

Fig 2. Measurement setup for air-gap torque

A four-channel, dc to 175 MHz, digital storage scope is used. It has a GPIB (IEEE488) input/output interface capability. Maximum sample rate is 100 megasample per second, per channel at 5 ms/div. Its storage capacity is 4 x 10 k.

Sample time differences among different channels are neglected in this study. This can be included easily if the specific time differences are given; however, when the time increment for sampling is small, the error relating to the time differences is negligible.

B. Air-Gap-Torque Measurement of an Adjusted-Speed Brushless DC Motor

The air-gap torque includes pulsating and fluctuating torque components that are affected by armature currents. A 1-hp, 4-pole, 230-V, three-phase brushless dc permanent-magnet motor is fed by an adjustable-frequency inverter. The motor is coupled to an eddy-current-disk load with torque gauge.

The output of the inverter is extremely unbalanced due to defective hardware inside the inverter. Since one

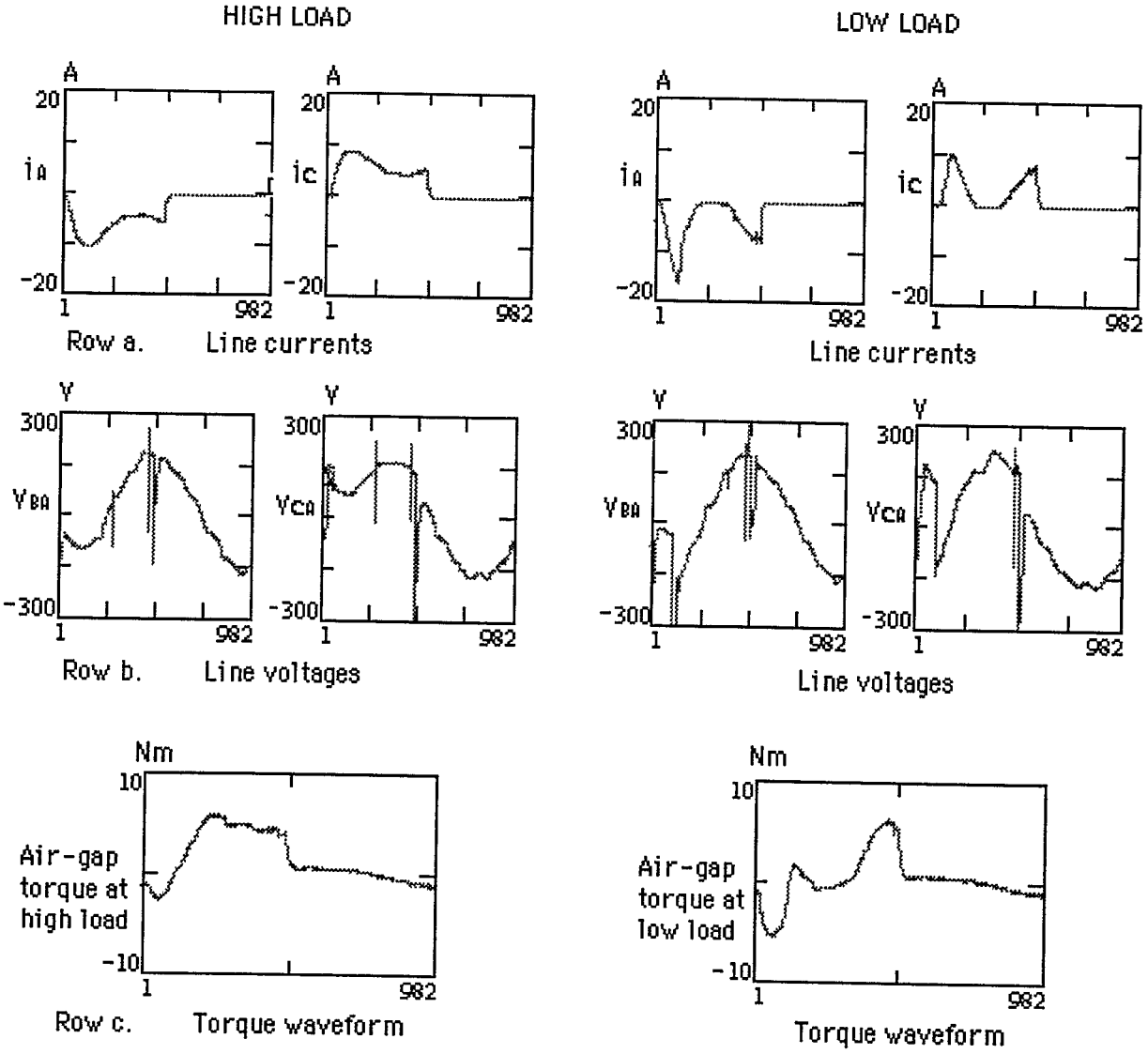

Fig. 3. Current, voltage, flux linkage, and air-gap torque waveforms (with 982 data points per cycle)

objective is to examine the air-gap torque measurement method that includes the situation of an unbalanced supply, the defective inverter is used.

Tests with high and low loads, respectively, are conducted without decoupling the motor. The high load refers to the highest possible load under unbalanced supply, which is 172 watts, and the low load is 5 watts. Both tests are at 1550 rpm.

Measured waveforms of one cycle for the high and the low loads are placed side by side in Fig. 3. The left two columns are for the high load and the right two columns are for the low load.

The first row (row a) of Fig. 3 shows the line currents i_A and ic. They contain dc components caused by the defective inverter. The current waveforms under high load look relatively square. The waveforms under the low load situation contain two bumps in each cycle of current. This indicates greater higher-order harmonics. The three phase currents are extremely unbalanced. Phase b current, which is the negative summation of i_A and ic, is nearly zero.

The harmonic current components for both the high and low loads, respectively, are listed in Table 4. The bold face numbers indicate the harmonic values that are obviously greater than the rest. According to the description given earlier in section III B, the predicted major frequencies of pulsating torques produced by all the current components shown in Table 4 and the fundamental winding component alone are given in bold face numbers in the right column of the same table. The expected major torque harmonic frequencies are 1ω, 2ω, and 4ω. The effects of other winding harmonic components can be evaluated in like manner.

Stator-current harmonics of experimental motor				
Order of current harmonics	Amplitude [amps]		Relative sequence of three phases	Sample torque freq. by fund. winding only
	High load	Low load		
dc	**3.45**	**2.64**	Stationary	1ω
1	2.15	0.75	Positive	dc
	2.48	**1.43**	Negative	**2ω**
2	0.61	**1.36**	Positive	**1ω**
	0.87	1.07	Negative	3ω
3	**0.92**	**1.50**	Positive	**2ω**
	0.96	**1.89**	Negative	**4ω**
4	0.39	0.23	Positive	3ω
	0.53	0.80	Negative	5ω
5	0.36	0.79	Positive	4ω
	0.25	0.94	Negative	6ω
6	0.33	0.41	Positive	5ω
	0.29	0.83	Negative	7ω
7	0.10	0.28	Positive	6ω
	0.13	0.35	Negative	8ω
8	0.23	0.29	Positive	7ω
	0.27	0.49	Negative	9ω
9	0.05	0.11	Positive	8ω
	0.01	0.07	Negative	10ω
10	0.16	0.26	Positive	9ω
	0.21	0.27	Negative	11ω
11	0.04	0.06	Positive	10ω
	0.06	0.10	Negative	12ω

Table 4 Stator-current harmonics of experimental motor and expected significant frequencies of torque

The second row (row b) of Fig. 3 presents line voltages V_{BA} and V_{CA}. The voltages at the low load appear to have more notches than the voltages under highest load. Consequently, higher harmonic magnitudes are associated with the low load situation.

Air-gap torque harmonics of experimental motor		
Torque harmonic frequency	Amplitude [Nm]	
	High load	Low load
dc	1.54	0.41
1ω	**2.88**	**2.41**
2ω	**1.47**	**1.05**
3ω	0.42	0.93
4ω	**0.72**	**1.39**
5ω	0.31	0.36
6ω	0.18	0.76
7ω	0.15	0.54
8ω	0.17	0.35
9ω	0.20	0.35
10ω	0.05	0.04
11ω	0.10	0.17

Table 5 Tested air-gap torque harmonics of experimental motor

The last row (row c) of Fig. 3 illustrates the tested air-gap torque waveforms calculated from (5). The harmonic contents of the tested torque waveforms are listed in Table 5. The significant harmonic frequencies are agreeable with those predicted frequencies given in Table 4. It is also expected that, as shown in Table 5, the higher order of torque harmonics under low load are more significant than those under high load.

IV. Conclusions

1) Torque ripple of a permanent-magnet motor can be classified into four types of torques according to the nature of their origin.

2) The four types are pulsating torques, fluctuating torques, reluctance cogging torques, and inertia and mechanical-system torques.

3) Pulsating torque is generated by the interactions between stator and rotor fields having the same number of poles, but rotating at different speeds.

4) Pulsating torques are inherently produced by the trapezoidal back-emf's and trapezoidal currents used in certain permanent-magnet adjustable-speed motors.

5) The torque ripples caused by pulsating torques may be reduced by purposely produced fluctuating counter torques.

6) Reluctance cogging torque is produced even when the motor is not energized, and can be measured when the motor is not energized.

7) Inertia and mechanical-system torques are generated by the dynamic motions of the mechanical components of motor. They are affected by the driven device.

8) Air-gap torque measurements for pulsating and fluctuating torques are conducted on a sample motor.

9) Experimental results agree with theoretical expectations.

V. Acknowledgments

The authors would like to thank the Oak Ridge National Laboratory (ORNL) for the support staff and facilities provided for the research work. The funding provided for the research is deeply appreciated. The authors would also like to acknowledge the earlier study done by Mr. Anthony Lopez [20] on brushless dc motors.

VI. References

[1] Vlado Ostovic, Istarska B. Osijck, "Computation of Saturated Permanent Magnet AC Motor Performance by Means of Magnetic Circuits," IEEE Paper No. CH2272-3/86/0000-0794, 1986 IEEE. p.p. 794-799.

[2] Alexander Levran, Enrico Levi, "Design of Polyphase Motors with PM Excitation," IEEE Transactions on Magnetics, Vol, Mag-20, No. 3, May 1984, p.p. 507515.

[3] Jaime De La Ree, Nady Boules, "Torque Production in Permanent-Magnet Synchronous Motors," IEEE Paper No. CH2499-2/87/000-0015, 1987 IEEE, p.p. 15-20.

[4] Touzhu Li, Gordon Slemon, "Reduction of Cogging Torque in Permanent Magnet Motors," *IEEE Transactions on Magnets*, Vol. 24, No. 6, November 1988, p.p. 2901-2903.

[5] Renato Carlson, Michel Lajoie-Mazenc, Joao C. dos S. Fagundes, "Analysis of Torque Ripple due to Phase Commutation in Brushless DC Machines," IEEE Paper No. 90/CH 2935-5/90/0000-0287, 1990 IEEE, p.p. 287-292.

[6] Ming-De Chen, Enrico Levi, Mark Dov Pelka, "Iron Saturation Effects in PM AC Motors," *IEEE Transactions on Magnetics*, Vol. Mag-21, No. 3, May 1985, p.p. 1262-1265.

[7] A. E. Fitzgerald, Charles Kingsley, Jr., Stephen D. Umans, Electric Machinery, p.546, McGraw-Hill Book Company, New York, 1983.

[8] Jing-Tak Kao, ANALYSES OF TRANSIENTS AND OPERATIONS OF ALTERNATING-CURRENT MACHINES, Second Edition, Science Press, Beijing, China, Sept., 1964.

[9] J.O. Ojo, V. Ostovic, T.A. Lipo, and J.C. White, "Measurement and Computation of Starting Torque Pulsations of Salient Pole Synchronous Motors," IEEE/PES 1989 Summer Meeting, Long Beach, California, July 9-14, 1989. Paper No. 89 SM 756-8 EC.

[10] J.S. Hsu, H.H. Woodson, and W.F. Weldon, "Possible Errors in Measurement of Air-Gap Torque Pulsations of Induction Motors," *IEEE Transactions on Energy Conversion* , (Paper No. 91 SM 390-5 EC).

[11] Jaime De La Ree, Jaime Latorre, "Permanent Magnets Torque Considerations," IEEE Paper No. 88CH2565-0/88/0000-0032, 1988 IEEE. p.p. 32-37.

[12] Eljas G. Strangas, Tuhin Ray, "Combining Field and Circuit Equations for The Analysis of Permanent Magnet AC Motor Drives," IEEE Paper No. 88CH2565-0/88/0000-0007, 1988 IEEE, p.p. 7-10.

[13] H. R. Bolton, Y. D. Liu, N. M. Mallinson, "Investigation into A Class of Brushless DC Motor with Quasisquare Voltages and Currents," *IEE Proceedings*, Vol. 133, Pt. B, No. 2, March 1986, p.p. 103-111.

[14] H. R. Bolton, R. A. Ashen, "Influence of Motor Design and Feed-Current Waveform on Torque Ripple in Brushless DC Drives," *IEE Proceedings*, Vol.131, Pt. B, No. 3, May 1984.

[15] Yoshihiro Murai, Yoshihiro Kawase, Kazuharu Ohashi, Kazuo Nagatake, Kyugo Okuyama, "Torque Ripple Improvement for Brushless DC Minature Motors," IEEE Paper No. CH2499-2/87/000-0021, 1987 IEEE, p.p. 21-26.

[16] Tomy Sebastian, Gordon R. Slemon, "Operating Limits of Inverter-Driven Permanent Magnet Motor Drives," *IEEE Transactions on Industry Applications*, Vol. 1A-23, No. 2, March/April 1987, p.p. 327-333.

[17] S. Funabiki, T. Himei, "Estimation of Torque Pulsation due to The Behaviour of A Convertor and An Inverter in A Brushless DC -Drive System," *IEE Proceedings*, Vol. 132, Pt. B, No. 4, July 1985, p.p. 215-222.

[18] John S. Hsu (Htsui), "Monitoring of Defects in Induction Motors Through Air-Gap Torque Observation," Paper No. 94A11, (EMC94-31), IEEE-IAS Annual Meeting, Denver, Colorado, USA, October 2-7, 1994.

[19] J.S. Hsu (Htsui), A.M.A. Amin, "Torque Calculations of Current-Source Induction Machines Using the 1-2-0 Coordinate System," *IEEE Transactions on Industrial Electronics*, vol. 37, no. 1, February, 1990, pp. 34 - 40.

[20] Anthony Lopez, "Brushless DC Motor," Study Report, Oak Ridge National Laboratory, 1994.

John S. Hsu (Htsui) (SMIEEE) is a senior staff scientist of the Digital and Power Electronics Group, Oak Ridge National Laboratory. He worked for Emerson Electric Company, Westinghouse Electric Corporation, and later for the University of Texas at Austin. Dr. Hsu has published many technical papers and holds seven patents in the area of rotating machines and power electronics.

Brian P. Scoggins is currently completing a one-year stay at Oak Ridge National Laboratory. He is a senior attending the University of Southern Indiana majoring in Electrical Engineering Technology.

Mr. Scoggins is a member of the USI Presidential Scholar's program and the Tau Alpha Pi honor society as well as a 1990 National Merit Scholarship Finalist, high school valedictorian, and former page for the Indiana State Senate.

Dr. Matthew Scudiere holds degrees in Physics from Kent State University and Nuclear Engineering from the University of Virginia. He has worked as a research scientist and inventor for most of his career in areas such as power electronics, permanent magnet motor design, and image and signal processing, and has 20 years' experience in instrumentation design and control. Matt has several awards from Martin Marietta for inventions and special achievements, and has several patents currently being processed as well as approximately 15 refereed papers published.

Laura D. Marlino received her Bachelor's degree in Electronics Engineering from the University of New Mexico in December of 1982 and her Master's from the University of Tennessee in 1991. Her industrial experience includes employment with Teledyne Camera Systems of Arcadia, California in 1983 and Honeywell Marine and Defense Systems in Albuquerque, New Mexico from 1983-1989. She is currently a staff engineer with the Power Electronics and Digital Systems Group at the Oak Ridge National Laboratory in Oak Ridge, Tennessee.

Donald J. Adams leads the Digital & Power Electronics Group at the Oak Ridge National Laboratory where he has been employed since 1977. He received a B.S. in Mechanical Engineering from the University of Mississippi in 1973 and a M.S. from the University of Tennessee in 1977. His work experience primarily includes process engineering, rotor dynamics, and power electronics. Don is a registered professional engineer in Tennessee.

Pragasen Pillay (SMIEEE) is an Associate Professor at the University of New Orleans, having obtained the Ph.D from VPI&SU in 1987 while funded by a Fulbright Scholarship. He is active in the IEEE, and he spent the summer of 1994 at the Oak Ridge National Laboratory as a faculty research participant.